Annu. Rev. Earth Planet. Sci. 2000. 28:539–70

SPREADING VOLCANOES[1]

Andrea Borgia[2], Paul T. Delaney[3], and Roger P. Denlinger[4]

[2]via di Fioranello 31, Roma 00134, Italia, 39.06.793.40443, fax 39.06.793.40072; e-mail: andrea@borgia.net

[3]U.S. Geological Survey, 2255 North Gemini Dr., Flagstaff, Arizona 86001, 520–556–7270, fax 520.556.7169; e-mail: delaney@usgs.gov

[4]U.S. Geological Survey, 5400 MacArthur Blvd., Vancouver, Washington 98661, 360–993–8904; e-mail: roger@usgs.gov

Key Words volcano structure, earthquakes, deformation, spreading, landslides, flank instability

■ **Abstract** As volcanoes grow, they become ever heavier. Unlike mountains exhumed by erosion of rocks that generally were lithified at depth, volcanoes typically are built of poorly consolidated rocks that may be further weakened by hydrothermal alteration. The substrates upon which volcanoes rest, moreover, are often sediments lithified by no more than the weight of the volcanic overburden. It is not surprising, therefore, that volcanic deformation includes—and in the long term is often dominated by—spreading motions that translate subsidence near volcanic summits to outward horizontal displacements around the flanks and peripheries. We review examples of volcanic spreading and go on to derive approximate expressions for the time volcanoes require to deform by spreading on weak substrates. We also demonstrate that shear stresses that drive low-angle thrust faulting from beneath volcanic constructs have maxima at volcanic peripheries, just where such faults are seen to emerge. Finally, we establish a theoretical basis for experimentally derived scalings that delineate volcanoes that spread from those that do not.

INTRODUCTION

Volcanoes pose many dangers in addition to their possible eruption. Most, for instance, are susceptible to landslides, large slumps, and debris avalanches. Large volcanoes occasionally generate damaging earthquakes, and in oceanic settings, tsunamis present an additional risk. In fact, many composite volcanoes and all of the earth's largest volcanoes undergo structural adjustments in response to their increasing size and weight. Commonly, these adjustments originate from deep

[1]The US Government has the right to retain a nonexclusive, royalty-free license in and to any copyright covering this paper.

within the volcanoes' edifices and even from their substrates. Although the deformations involve settling or collapse of upper slopes and summits of volcanoes, they ultimately produce horizontal motion along their distal slopes and even beyond. Accordingly, we recognize these deformations collectively by the process of volcanic spreading. To a great extent, this term encompasses the structural dynamics of volcanoes.

Van Bemmelen (1949) was the first to emphasize that volcanoes, as they evolve through numerous intervals of eruption, undergo a form of mountain building. Although most mountains grow by uplift and differential erosion of lithified rocks brought from depth, volcanoes grow by accumulation of new deposits that are generally poorly lithified and may rest upon substrates that are similarly weak. The ever-increasing height and weight of volcanic mountains is then made more precarious by poor consolidation of the constituent deposits, especially in view of the hydrothermal alteration that weakens rocks subjected to moderately high temperatures. Although significant horizontal motions of volcanoes are most often manifested by co-eruptive sector collapses, such as occurred at Mount St. Helens in 1980 (Lipman & Mullineaux 1981, Francis & Self 1987, Siebert 1992), and by giant landslides, such as those of the submarine slopes of Hawaii (Moore et al 1994), the generally slower spreading motions along deeply seated structures that prevail at most volcanoes are the focus of this paper. Perspectives and many case examples of the causes and effects of volcano flank instability can be gained from several recent compilations (McGuire et al 1996, Elsworth 2000).

Van Bemmelen (1949) focused on problems of contemporary orogeny, volcanism, and sedimentation along the archipelagos of the East Indies, present-day Indonesia, Malaysia, Philippines, and New Guinea. He was struck not only by the well-known association of earthquakes and volcanoes, but also by the deformations on and around many of the volcanoes themselves. At the Indonesian volcanoes Merapi, Soropati, Lawu, ArdjunoWelirang (Figure 1), Tjareme, Bukittunggul, and Tjanggak, Van Bemmelen recognized fault scarps across large sectors of their edifices; he also documented anticlinal ridges and thrusts along and beyond their peripheries. These volcanoes are built on thick sections of marine clays and fine-grained Plio-Pleistocene deposits, so these deformation structures were attributed to faulting and flow of sediments from beneath the volcanoes in response to gravitational loading. To connect these observed structures, he hypothesized low-angle faults—decollements or detachment surfaces in today's parlance—that extended from the upper slopes of volcanoes to the sedimentary substrate (Figure 1) and thus transported by gravity the volcanic overburden toward the adjacent basins. These original observations have been extended and amplified over the years through monitoring of active volcanoes and investigations into their structure and evolution, as well as geologic mapping of extinct volcanoes now dissected by erosion; debris avalanches, for instance, are now recognized at many of the volcanoes studied by van Bemmelen.

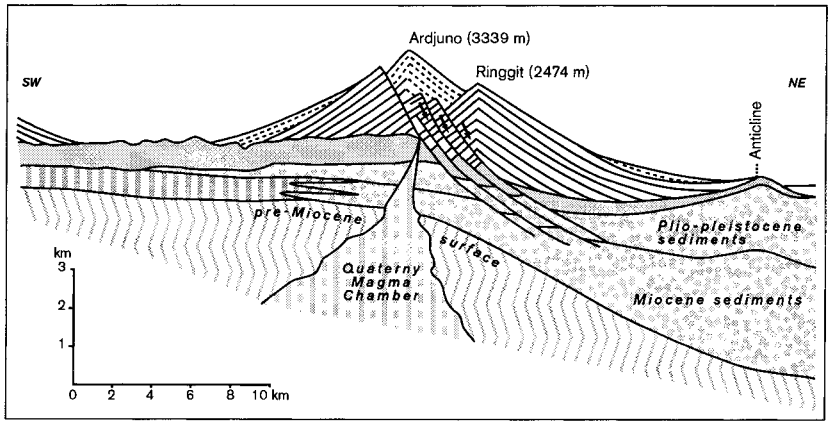

Figure 1 Example of volcanic spreading as envisioned by Van Bemmelen: a cross section of Ardjuno volcano showing inferred imbricate slip surfaces of volcanic collapse extending into underlying Plio-Pleistocene and Miocene sediments with distal anticlinal folds. In this and other maps and sections of other Indonesian volcanoes, extensional deformations in volcanic highlands were closely related to compressional structures of the distal flank and underlying sedimentary strata; the anticline northeast of Ardjuno deforms older volcanic deposits and is generally contemporaneous with the faulting exposed on the southern flank of that volcano. The underlying sediments were thought to comprise a ''bad foundation'' or ''plastic foundation.'' After Van Bemmelen (1949).

SPREADING VOLCANOES

A volcano is far more complex than is implied by its classical definition of ''a vent through which magma and associated gases and ash erupt'' (Jackson 1997). They all possess considerable heterogeneity and internal structure. Moreover, the internal and underlying systems of magma reservoirs, fractures, faults, and folds, groundwater aquifers, and so forth are crucial components of the volcanic environment and strongly affect the evolution of all composite volcanoes.

Spreading is the result of that set of processes that produce irreversible horizontal outward displacements on the slopes and peripheries of volcanoes and in the nearby substrate. Why does this occur? As volcanoes deposit their ejecta and lavas, they also gain potential energy. They grow higher and become heavier. A magma reservoir may develop within the edifice and exert a considerable internal force. There's always a possibility of structural failure. When this occurs, a volcano's summit or upper flanks subside as material moves outward toward the periphery. Spreading, then, is a natural response that tends to decrease the potential energy that exists in volcanic edifices.

Most spreading encompasses a vertical scale comparable to the height of a volcanic edifice. Therefore, while sector collapses and shallow landslides result

in horizontal transport toward the volcanic periphery, we view them as rather superficial. Stated somewhat differently, landslides and sector collapses may be viewed as processes that result from volcanoes that are growing too fast to spread effectively by other means.

Spreading is controlled by two primary mechanisms—faulting and flow—acting within the volcanic edifice. Faulting may also be important at the base of the edifice; spreading is facilitated at many oceanic volcanoes, for instance, by basal decollements. Faulting and flow may also be important beneath volcanoes that rest upon clay and other weak sediments; we review several examples in the next section. Volcanoes may spread by sector collapses and by superficial wasting processes if they rest upon strong, intact rocks, lack basal decollements, and possess a high degree of internal strength.

Spreading is not an eruptive phenomenon, though it may be related to events that include eruptions; many, if not most, sector collapses appear to be co-eruptive, for instance. The largely reversible process of magma-reservoir inflation and deflation makes no net contribution to spreading, although associated dike intrusion may. Co-eruptive summit collapse, even if associated with caldera formation, also makes no contribution to spreading.

EXAMPLES

We use, as examples of spreading processes, observations collected from a number of volcanoes, emphasizing at each the origin of, and factors contributing to, the spreading deformations. We note especially the Nicaraguan spreading stratovolcanoes Mombacho, Concepciòn, and Maderas compared by Van Wyk de Vries & Borgia (1996) with nearby volcanoes, San Cristobal (Figure 2*a*) and Casita, which do not spread. They all stand 1400–1800 m above relatively flat plains and have diameters of 9–16 km. We then examine several volcanic fields flanked by thrust belts that extend beneath them, before turning to several volcanoes that display combinations of debris-avalanche and deeper spreading processes.

Mombacho, Nicaragua: Faulting of the Edifice

Mombacho volcano, which last erupted less than a thousand years ago, displays several prominent sector collapses as evidenced by breakaway scarps and debris-avalanche deposits (Figure 3*a*). It also exhibits several concentric scarps along its lower flanks that are interpreted as the toes of thrusts. The largest of these, on the east flank, has about 100 m of uplift. Mombacho is built on a section of well-lithified ignimbrites and Tertiary marine flysch. It also displays considerable hydrothermal and fumarolic activity, which presumably alters and weakens it. The combination of the sector collapse scarps on the upper slopes and the thrusts on the lower slopes implies that deformation of the volcano is confined largely

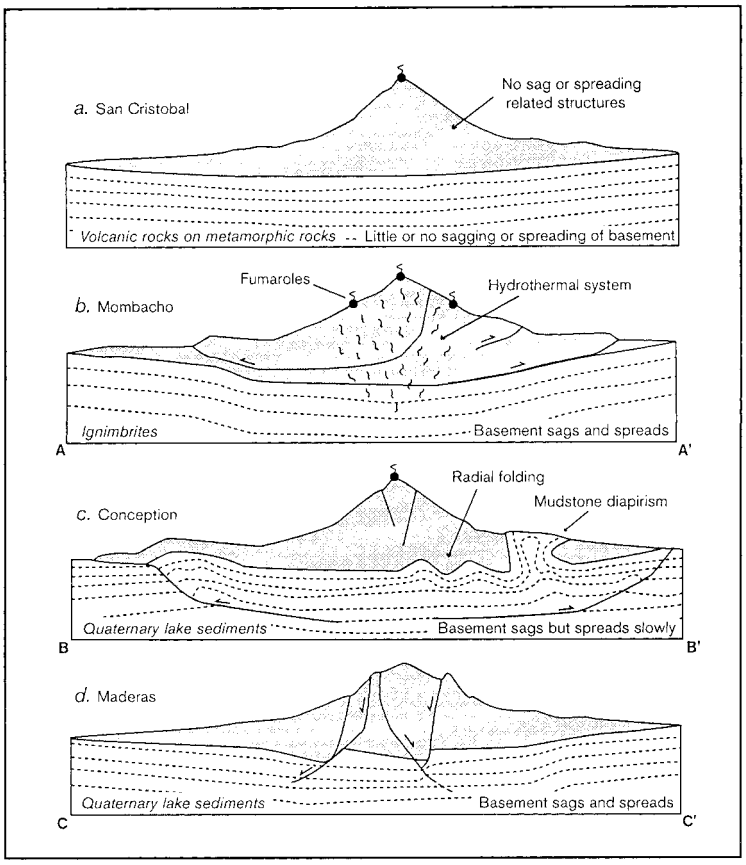

Figure 2 Sections across Nicaraguan volcanoes San Cristobal (*a*), Mombacho (*b*), Concepción (*c*), and Maderas (*d*). After Van Wyk de Vries & Borgia (1996).

to its edifice, recording upslope collapse and extension and downslope contraction and uplift (Figure 2*b*).

Importantly, the substrate beneath Mombacho is considerably more coherent than that beneath the following examples, Concepciòn and Maderas.

Concepción and Maderas, Nicaragua: Faulting and Flow of the Edifice, Faulting and Flow of the Substrate

Concepción and Maderas volcanoes are greatly deformed (Figures 2*c*,*d*, 3*b*,*c*) owing to weak Quaternary clayey sediments of Lake Nicaragua, upon which they are built. Although the former volcano last erupted about 45 years ago and dis-

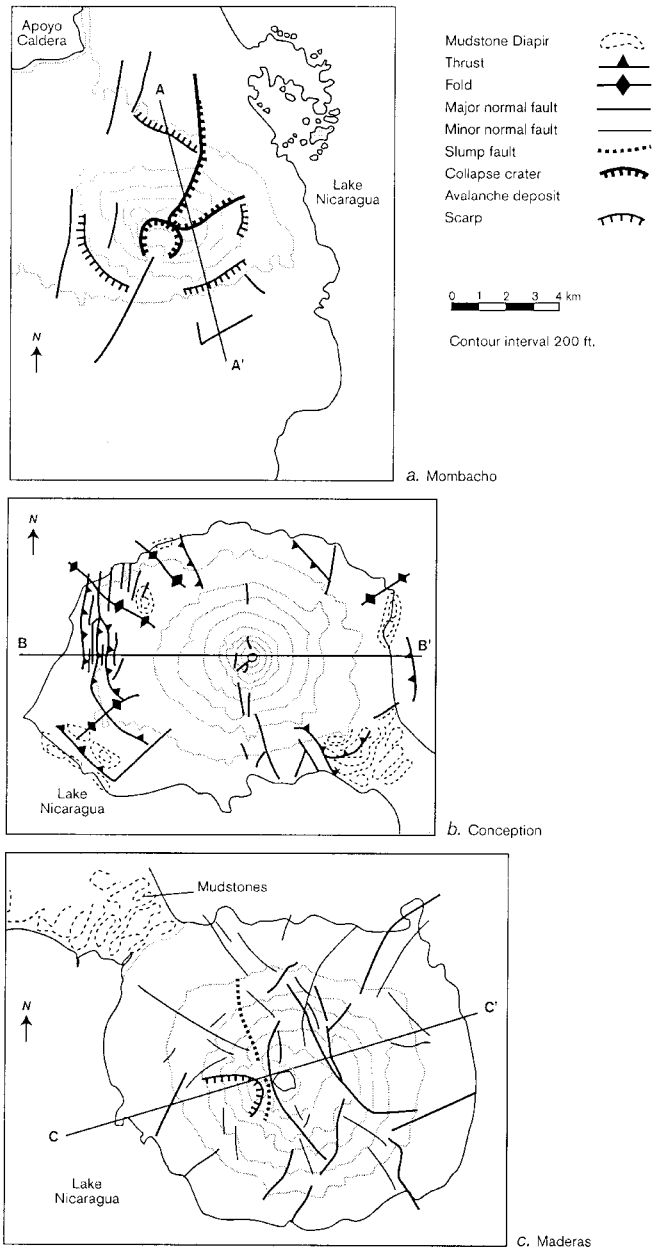

Figure 3 Structure maps of Nicaraguan volcanoes Mombacho (*a*), Concepción (*b*), and Maderas (*c*). After Van Wyk de Vries & Borgia (1996).

plays mild fumarolic activity at its summit, the latter has been dormant for more than 3 ka.

While minor slumping has occurred on the north flank of Concepción, fissures span the stratocone irregularly from north to south across its summit (Figures 2*c*, 3*b*); sited along them are spatter and cinder cones, eruptive fissures, and maars. The lower slopes possess concentric thrust faults and radial folds, with minor normal faulting. Several of the folds can be traced into the sediments of Lake Nicaragua, and a thrust fault on the east side of the volcano emerges in those sediments. Elsewhere around the periphery of Concepción, lake sediments are uplifted. Additionally, the lower slopes are pierced in the eastern sector by diapirs of the underlying mud deposits. Taken together, these features demonstrate that deformation of Concepción originates in its substrate, which has moved out from beneath it. The deformation is sufficiently rapid that the summit appears to have an average extension rate of about 5 cm/yr.

Maderas is traversed by many high-angle normal faults, which form a complex horst-and-graben structure dominated by an irregular graben oriented north-south across the summit (Van Wyk de Vries & Merle 1996). Several of the faults extend into the adjacent lake sediments, where displacements lessen and deformation appears to have been ductile. Some slumping has occurred on the southwest flank, demonstrated by semicircular scarps with up to approximately 100 m of displacement.

Involvement of the substrate in the deformation of Concepción and Maderas is unambiguous. It is also not surprising, in view of the unlithified character of the muds and volcanic sandstones of Lake Nicaragua. Van Wyk de Vries & Borgia (1996) demonstrated with elasto-plastic models that maximum stress differences beneath the idealized volcanoes exceed 100 MPa, well beyond the shear strength of rocks considerably more indurated than the sediments of Lake Nicaragua. Because each volcano is approximately 10 km in diameter and 1500 m high, the nominal load on the substrate beneath them exceeds 15 MPa (probably around 45 MPa beneath the summits). We infer that horizontal stress gradients from the center to the periphery are therefore in the order of 10 MPa/km.

Tharsis Tholus, Mars: Faulting of the Edifice, Faulting and Flow of the Substrate

Tholus (Figure 4) is a Martian volcano of the Tharsis region; it is more than 100 km wide in its shortest aerial dimension. This volcano is dissected by arcuate scarps distributed over its flank and summit (Crumpler et al 1996). Several scarps merge with the caldera walls, which are nested and also cut by scarps that extend outward to the flanks. Other scarps resemble sector-collapse structures, for instance along the southwest quadrant of Tharsis Tholus (Figure 4). Taken together, these scarps record a series of spreading episodes that span at least the intervals between and after the formation of the nested calderas. Tharsis Tholus is surrounded by younger lavas that cover its lower slopes, thus hiding spreading

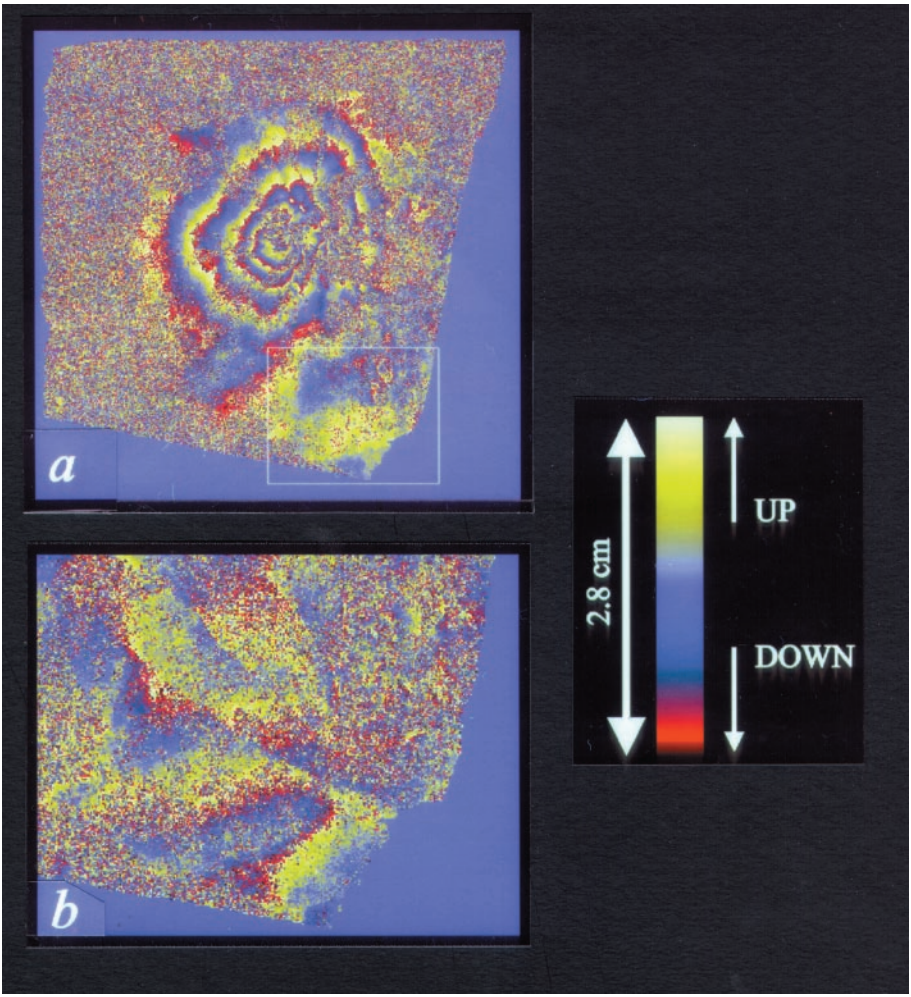

Figure 10 Satellite synthetic aperture radar interferometry images of Mount Etna, Sicily. (*a*) Image for August 1993 to October 1995 dominated by about 10 cm of pre-eruptive inflationary motion about the summit. Concentric deformation pattern is disturbed by spreading motions on the east and south flanks. Area of image is 55 km × 55 km. From Lanari et al (1998). (*b*) Image for October 1993 to December 1998 showing uplift in the 9 km × 15 km area around the city of Catania. The east-northeast trending bulge shows uplift of the basal anticline at Catania.

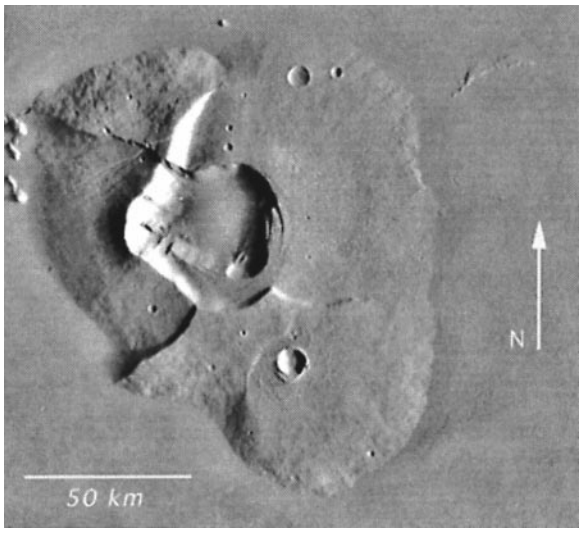

Figure 4 Multiple scarps intersecting nested caldera walls on Tharsis Tholus in the Tharsis region of Mars. Construct is about 120 × 150 km; the summit caldera is about 30 × 50 km. Lower slopes are covered by younger deposits. Location 13.5°N, 90.9°W. Viking Orbiter image 858A23.

structures that may be present around its periphery, although basal block faulting is present at its northeastern base. Comparing this with Maderas volcano (Figure 3*c*), we suspect the faulting extends through the Tholus edifice into a weak substrate that itself has deformed in response to the weight of volcanic overburden.

Marysvale Volcanic Center, Utah: Faulting of the Substrate

One of the most spectacular examples of low-angle thrust faulting transporting rocks from beneath a volcano is found around the 20–30-Ma-old Marysvale center of southern Utah (Lundin 1989, Merle et al 1993). There, subsequent erosion has exposed a series of thrust faults arranged concentrically about the southeast sector of the volcanic field (Figure 5). The faults bottom along evaporitic beds of the Jurassic Carmel Formation and extend upward to fault-propagated folds in deposits of Eocene age. Transport directions along the thrusts span almost 90° of southeasterly and southerly azimuths. Although the thrusts reveal crustal shortening where exposed, this form of thin-skinned tectonics apparently originates beneath the nearby volcanic sequence, centered 40–60 km to the northwest, because the thrusts bear no relation in either age or style to the nearby Sevier system. Rather, thrust-transport directions verge to a locus beneath the Marysvale center, which covers about 5,000 km^2 and has a maximum thickness in excess of 3,000 m. The Marysvale field is probably the best known example of a dissected, subvolcanic thrust system formed by gravitational loading.

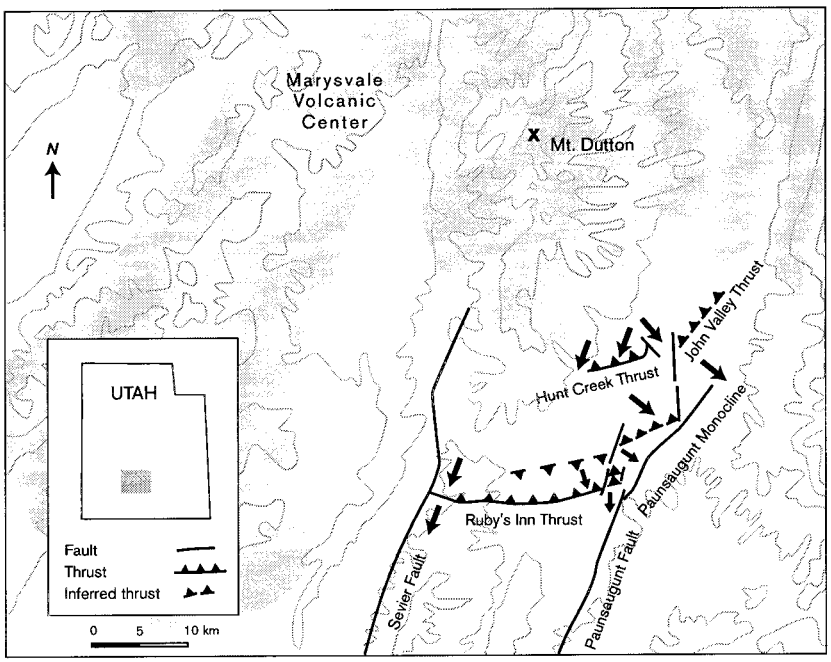

Figure 5 Marysvale volcanic field, southern Utah. This 20–30 Ma volcanic center and much of the underlying Mesozoic and Tertiary sediment around its periphery are now dissected by erosion, which also exposes both regional tectonic structures of the Sevier and Laramide orogenies and other structures—primarily thrust systems that sole into evaporitic layers of the Carmel Formation—having transport directions (*arrows*) radial from a locus of the Marysvale center near Mount Dutton. The thrusts deform Eocene strata and are probably coeval with formation of the Marysvale volcanics. After Lundin (1989) and Merle et al (1993).

Central Costa Rica Volcanic Range: Faulting of the Substrate

Thrust faults extending to the earth's surface from beneath active Quaternary volcanoes have also been documented on both sides of the highlands formed by the Costa Rican volcanoes Platanar, Poas, and Barva (Borgia et al 1990). Although Platanar has probably been quiescent for several thousand years, Poas last erupted about 50 years ago. The Central Costa Rica volcanic range (Figure 6*a*) rises from 1,000 to 2,000 m above its surroundings and is about 20 km wide. On both sides of the range are topographic ridges that parallel it. Where dissected by erosion or quarry operations, the ridges are viewed as the surface expressions of fault-propagation anticlinal folds and faults that accommodate horizontal-shortening

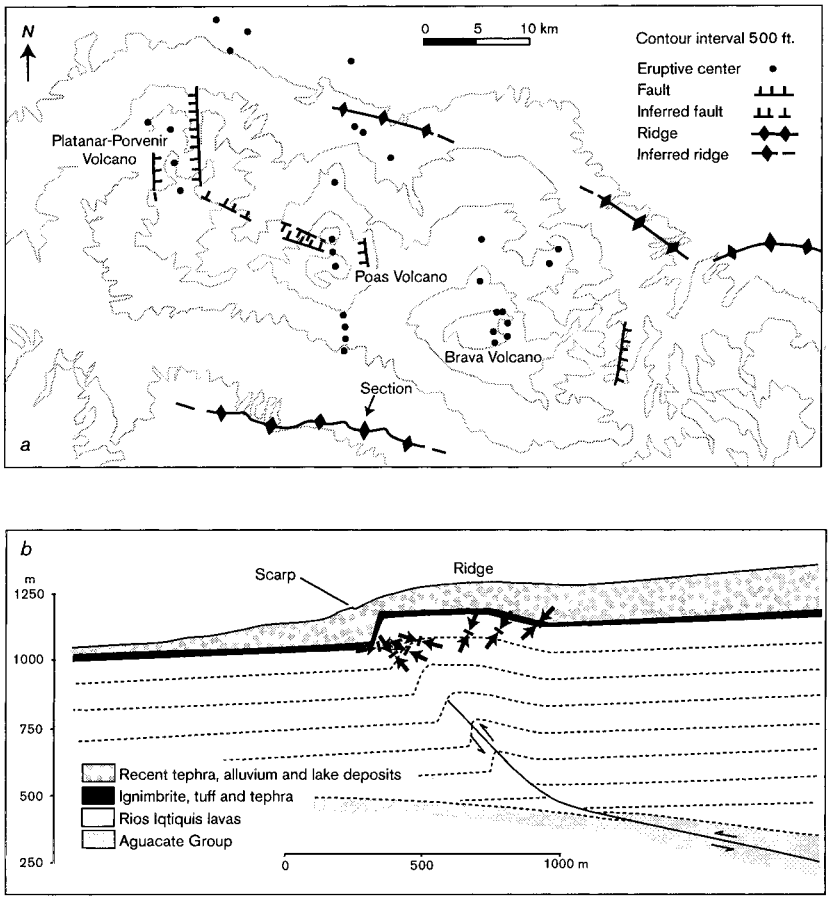

Figure 6 Northeast section of the Central Costa Rica volcanic range, showing Platanar, Poas, and Barva volcanoes. (*a*) Topography, eruptive centers, and generalized structure. (*b*) Section across topographic ridge on southwest side of the volcanic range. *Arrows* indicate directions of maximum stress calculated from field measurements of fault planes. After Borgia et al (1990).

motions (Figure 6*b*). The underlying thrust fault probably rises at a 15° angle from a detachment less than a kilometer beneath the volcanic products of Platanar, Poas, and Barva. As with many thrusts, the motion they induce near the earth's surface is distributed and manifested by asymmetric folding and distributed faulting. Diffuse, shallow earthquakes (largest recorded event is M = 6.6) that have focal mechanisms consistent with thrust motion suggest that spreading of the central Costa Rica volcanic range is contemporaneous. The slumping of the lower

flanks of Platanar, Poas, and Barva seems to be compensated by extension and formation of grabens along the range axis (Figure 6a; Prosser & Carr 1987).

Olympus Mons: Faulting of the Edifice, Faulting of the Substrate

The largest volcano in our solar system has also undergone spreading. Olympus Mons, on Mars, is truly enormous, rising about 22 km above the surrounding slopes of the Tharsis Rise and extending across a 700-km diameter. It possesses numerous terraces on its upper flanks, and its lower flanks end at prominent outward-facing scarps up to 8 km high (Figure 7). Morphologically, the scarps are complex (Borgia et al 1990); associated with them are basal wrinkle-ridges, horst-and-graben structures with blocks tilted toward the summit of the volcano, landslides, and other detachments. Upslope of the scarps, radially oriented normal faults can be found. Locally, the scarps are covered by younger lavas and cut by landslide scars. The scarp surrounding Olympus Mons has many interpretations. We favor a structural origin consistent with volcanic spreading, with the scarps underlain by thrust faults that extend from beneath the volcano, similar to the fault structures that extend beneath the Marysvale volcanics (Figure 5) and the central Costa Rica volcanic range (Figure 6).

The flank terraces on Olympus Mons (Figure 7) have also been interpreted as the surface expressions of underlying thrust faults (Thomas et al 1990). The scarps at the outsides of the terraces have a sharp break at their bases, and slope upward in gentle convex curves. This morphology is more likely the result of thrusting rather than normal faulting, which typically produces the sharpest break in slope at the top of a scarp. Interestingly, most of the terraces are around the mid-height of the volcano where slopes are steepest. An elastic model of gravitational stresses (Thomas et al 1990) showed that compressive radial stresses parallel to the volcano surface would be about 250 MPa, consistent with deformation by thrust faulting. It is also interesting that these high stresses are the result of both steep slopes and large volcano diameter. Consistent with this observation, the other Martian volcanoes known to exhibit flank terraces are Pavonis Mons, Ascraeus Mons, and Arsia Mons.

Although Olympus Mons lacks scallops or horseshoe-shaped valleys indicative of debris avalanches, the aureole deposits in the plain to the northwest are thought to be the result of such activity (Head 1996). The aureole deposits extend for up to 750 km from the basal scarps and comprise numerous landslides. Their asymmetric distribution about Olympus Mons is thought to result from the northwestward regional slope of the Tharsis Rise.

Piton de la Fournaise, Reunion Island: Faulting and Flow of the Edifice

At Piton de la Fournaise, dredging, bathymetry, and seafloor imaging (Figure 8) show that the subaerial, eastward-facing sector collapse has been formed by repeated landslides of subaerially deposited lavas (Labazuy 1996, De Voogd et

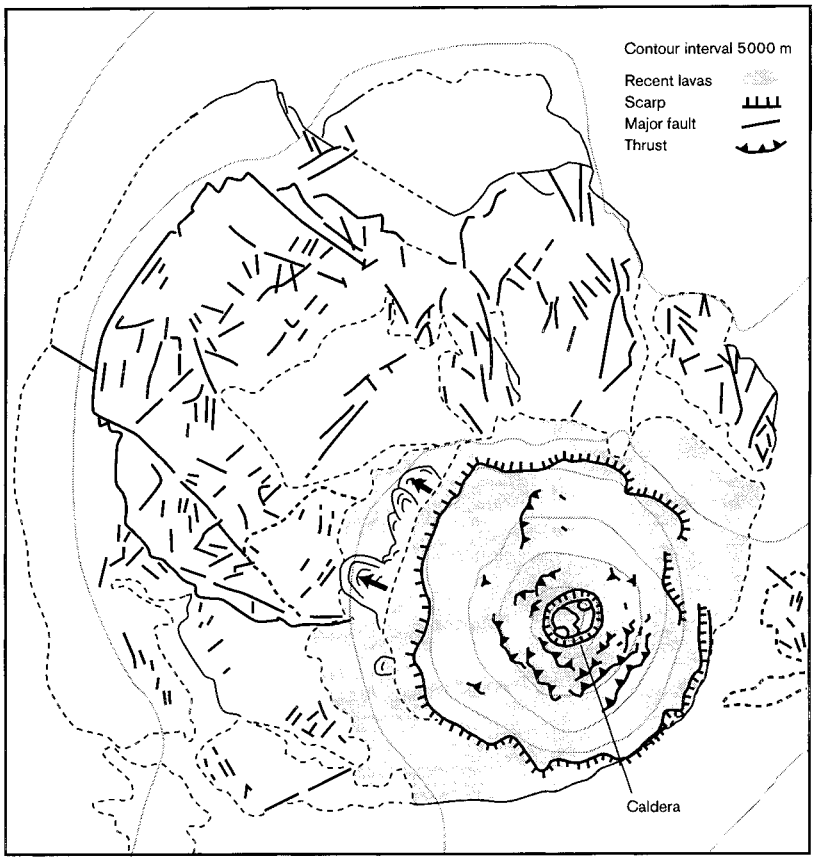

Figure 7 Olympus Mons. Stippled region shows younger lavas. Region northwest of Olympus Mons with numerous faults and ridges is the aureole deposit that consists of numerous landslides. Also shown is the outward-facing perimeter scarp and locations of the larger terrace faults on the slopes of Olympus Mons. After Thomas et al (1990) and Head (1996).

al 1999). The present-day collapse valley accounts for no more than 80 km^3 of the 550 km^3 of submarine landslide deposits. It follows that the submarine deposits record numerous intervals of sector collapse. Moreover, based on drill-hole data, it is thought that some sliding surfaces may be less than a kilometer below sea level (Labazuy 1996), which indicates debris-avalanche transport of subaerial deposits to the distal submarine fan. Seismic reflection data, on the other hand, offer evidence for multiple decollement surfaces (De Voogd et al 1999). Importantly, a prominent reflector and possible basal decollement occurs at the base of the edifice, which is built on oceanic sediments that average 600 m in thickness.

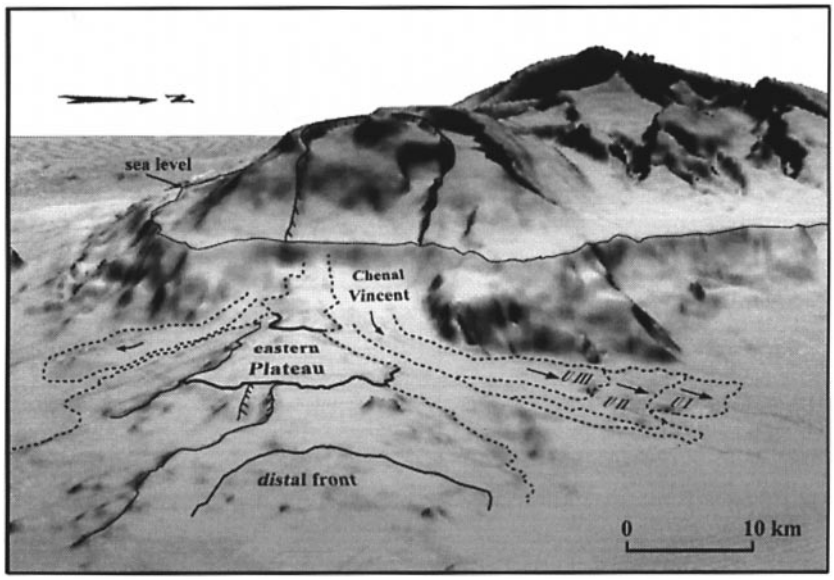

Figure 8 Three-dimensional view of Piton de la Fournaise, Reunion Island, showing multiple submarine debris avalanche deposits that emanate from the horseshoe-shaped valley scalloped into the east flank. Behind is Piton des Neiges, which evidently possesses structural blocks separated by valleys, a sign of through-going faults and volcanic spreading. From Labazuy (1996).

These sediments, much thicker than those beneath the island of Hawaii, probably serve as a weak layer for volcanic spreading that is presently masked by the more recent sector-collapse morphology. It appears, then, that Piton de la Fournaise transports debris to its periphery both by shallow debris-avalanches and by deeper, probably slower, slump motion. The structure of the older neighboring volcano Piton des Neiges (Figure 8) is apparently generated by block-faulting, tilting, and spreading.

Etna: Faulting of the Edifice, Faulting of the Basement

Like Piton de la Fournaise, Mount Etna (Figure 9*a*) possesses a large scalloped valley, the Valle del Bove, indicative of graben formation (Merle & Borgia 1996) and debris-avalanche activity (Guest et al 1984, Calvari et al 1998). The surface of Etna is significantly faulted (Rasà et al 1996, Rust & Neri 1996) on its eastern and southern slopes, however, with several fault zones dominating the production of earthquakes (Montalto et al 1996). More important, where exposed at the southern margin of Etna, the Pleistocene clays and basal lavas upon which Etna is built are tilted and uplifted more than 400 m (Borgia et al 1992). Outcrops of these rocks display thrust faults and related folds. Spreading of Etna southward

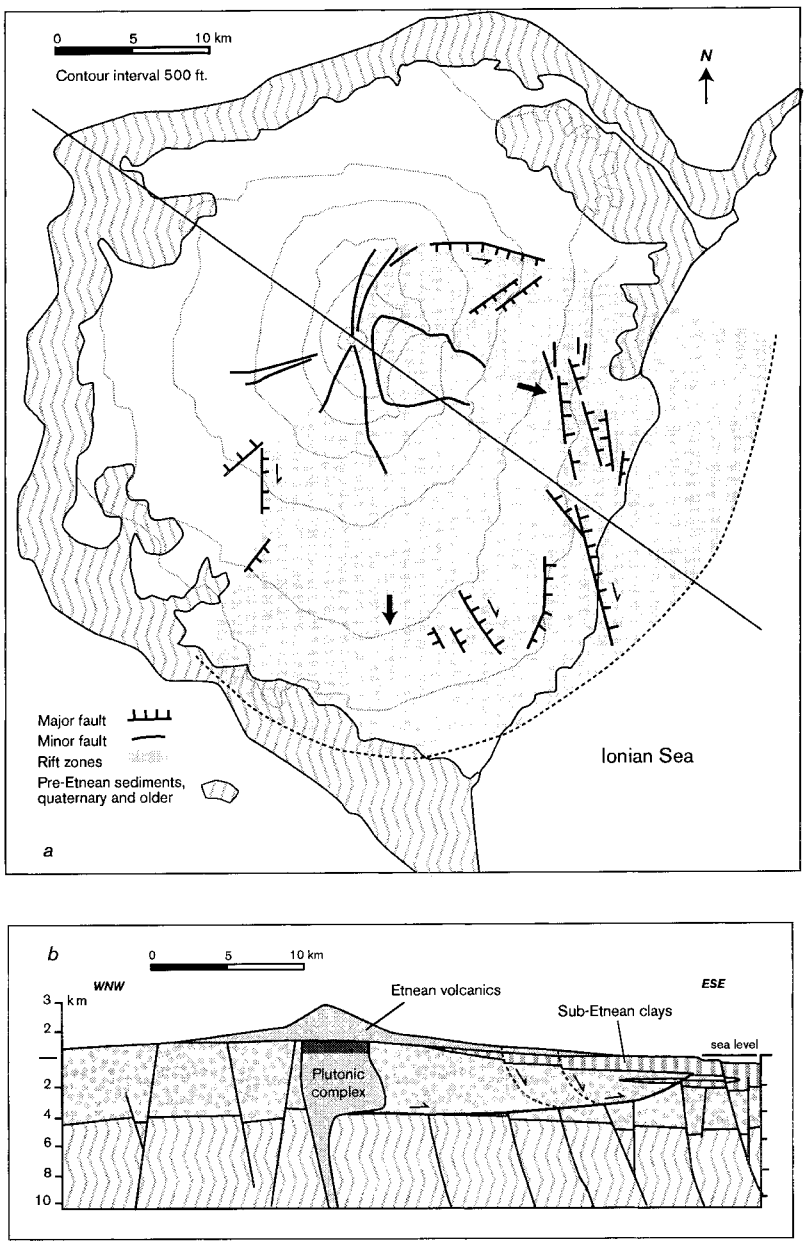

Figure 9 Mount Etna, Sicily. (*a*) Structural map showing faulting on the east flank, as well as the Valle del Bove, presumably the headwall area of a landslide complex. (*b*) North-south structure section across Etna, showing decollement in sub-etnean clays. After Borgia et al (1992) and Rasà et al (1996).

produces summit extension compensated by contractional deformations low on its slopes and beyond, with weak clays beneath as the transporting agent. Much of Etna's coastline behind the submarine ridge is uplifting at rates locally exceeding 1.5 mm/yr (Firth et al 1996). Spreading southward is measured by synthetic aperture radar interferometry (Figure 10, see color insert) and by global position system measurements to be about 0.7 cm/yr southeastward (Borgia et al 2000), consistent with that inferred for the past 80 ka (Borgia et al 1992). Many earthquakes at Mount Etna originate above its decollement and suggest a complex interaction among many structural blocks within the unbuttressed sectors (Montalto et al 1996).

Kilauea Volcano: Faulting and Flow of the Edifice, Basal Faulting, Rifting

The theme of this paper would have been no surprise to the ancient Hawaiians, apparently, because a literal translation of Kilauea is ''place of spreading.'' Indeed, Kilauea is pervaded by open ground cracks along most of its 80-km-long subaerial rift system; these episodes of rift-zone crack opening and fissure eruption undoubtedly prompted the volcano's Hawaiian name. Early volcanologists were drawn to the dikes, the magma-filled cracks that feed fissure eruptions, as the cause of seaward flank motion. The presence throughout the Hawaiian Islands of large seaward-facing escarpments, however, offered evidence of other, apparently more infrequent, processes manifested by slump blocks or folds (Moore et al 1994) related to basal-thrusting (Borgia et al 1990). Persistent, moderate-magnitude seismicity from beneath the south flank of Kilauea (Figure 11*a*), as well as occasional large earthquakes, also suggested that the volcano is mobile and unstable.

We now know that huge landslides and slumps extend hundreds of kilometers offshore around the islands, and that mass wasting is integral and recurrent (Moore et al 1994, Smith et al 1999). At Kilauea, the Hilina slump is in constant motion. The subaerial portion of the slump, the south flank, has been moving seaward at 6–10 cm/yr since 1983 (Delaney et al 1993, Owen et al 1995). For several years prior to 1983, it had been moving at rates of about 40 cm/yr (Delaney & Denlinger 1999), and it moved about 25 cm/yr (Delaney et al 1998) for several years after the magnitude 7.2 earthquake of 1975 (Lipman et al 1985)—the largest flank earthquake in Hawaii since the magnitude 8 event of 1868 (Wyss 1988).

Elastic dislocation models (Delaney et al 1993; Owen et al 1995, 2000) using geodetic data collected at Kilauea strongly suggest that the rift system detaches the south flank from the stable interior of the island of Hawaii (Figure 11*a*), just as the basal decollement detaches the flank from its substrate, which is ocean seafloor. By this interpretation, Kilauea's rift zones between about 6 and 9 km depth, adjacent to the mobile south flank, possess a tabular reservoir of magma and rock too hot to withstand a shear stress (Delaney et al 1990, Borgia & Treves 1992, Borgia 1994, Clague & Denlinger 1994, Clague 1995). Dike intrusions in

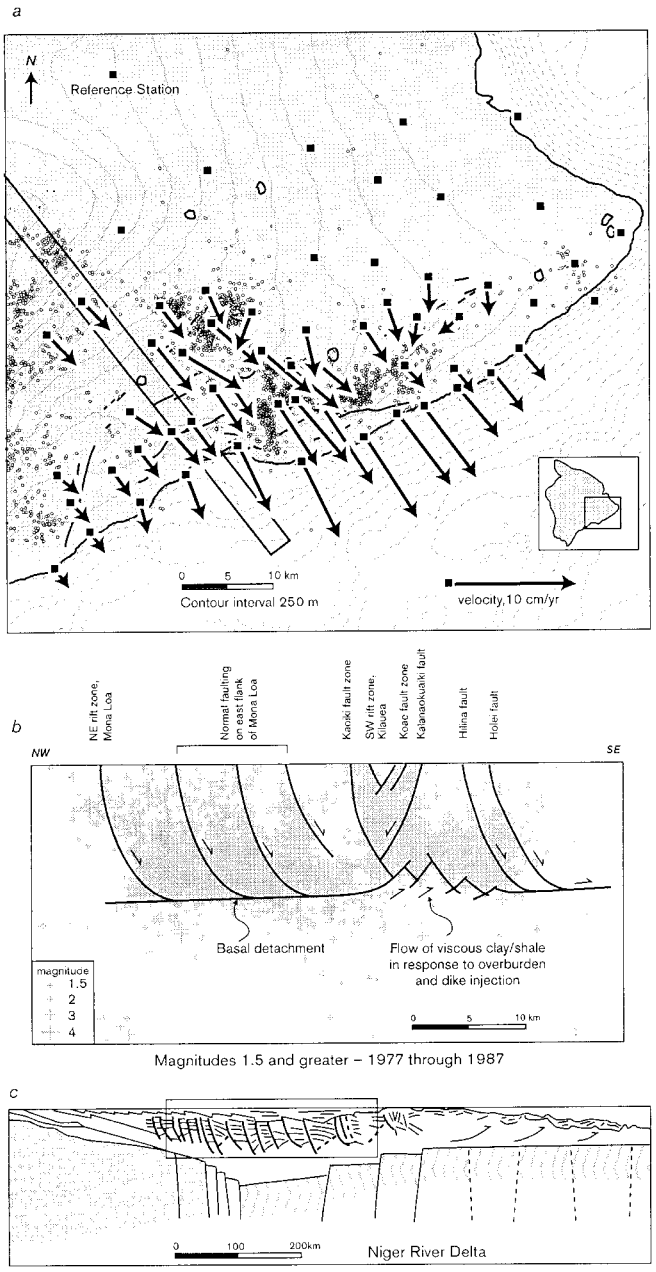

Figure 11 See legend on the next page.

the rift zone are seen as brittle, near-surface responses to rift-zone dilation and decollement fault creep already accumulated at depth (Delaney & Denlinger 1999).

Yet, Kilauea volcano possesses several systems of normal faults, the Hilina and the Koae, and is bounded by yet another, the Kaoiki. Whereas scarps of the Hilina and Kaoiki systems face seaward, those of the Koae system face in the opposite direction and have opening as well as dip-slip displacements (Denlinger & Okubo 1995). Synthesizing these observations of the surface geology with earthquake focii yields a structural reconstruction of Kilauea (Figure 11*b*). In this reconstruction, the low-angle basal detachment fault, or decollement, works in sympathy with normal faults and antithetic normal faults to accommodate extension and spreading in a fashion not unlike that observed in river deltas and other depositional wedges. The reconstruction relies on the analogy between volcanoes that grow by deposition of ash and lava and sedimentary deltas that grow by deposition of fine-grained clastic sediment (Figure 11*c*). Although drill-hole and seismic imaging data are sparse on volcanoes, they are abundant on the world's oil-rich deltas. In these settings extensional synthetic and antithetic listric normal faulting in proximal or upslope regions of deltas, associated with underlying ductile flow and diapirism, gives way to thrusting and nappe structures in the distal regions.

THEORY

Many of the processes inferred from the preceding field examples have been examined theoretically and experimentally. Failure of the edifices themselves has been examined from the point of view of limit-equilibrium wedges (Dieterich 1988, Iverson 1995). As applied to Hawaiian volcanoes, these treatments require basal pore-fluid pressures that are very nearly lithostatic, a condition that seems problematic for edifices that have been through many cycles of major earthquakes and mass-wasting events. Alternatively, models with viscous and elastic-viscous flanks (Borgia 1994, Delaney & Denlinger 1999) have met with some success,

←

Figure 11 Kilauea Volcano, Hawaii. (*a*) Map view showing distribution of earthquake epicenters and recent displacements determined by GPS data (Owen et al 2000), both for the interval from 1990 to 1996. Earthquakes are of magnitude greater than 2. Displacement gradients across the rift zones and summit are steep, indicating that the rift system is the major detachment of Kilauea's south flank from the rest of the Hawaiian volcanic pile. Also shown are rift zones and major fault zones. (*b*) Section across Kilauea, NNW-SSE, showing earthquake focii and inferred fault structures. Seismic volume used for this section is shown in *a* and uses well-located earthquakes between 1977 and 1987. (*c*) Section along the Niger River delta showing fault structures and flow structures similar to those hypothesized at Kilauea. After Evamy et al (1978).

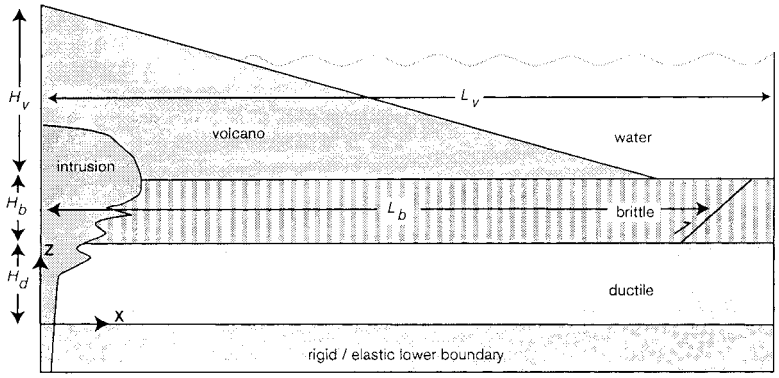

Figure 12 Schematic diagram of volcanic spreading parameters.

although they incorporate a poorly constrained and problematic property—the viscosity of the basal decollement or of the volcanic pile. The flow and faulting of volcanic substrates has been examined in scaled laboratory experiments (Merle & Vendeville 1995, Merle & Borgia 1996) and numerical models (Van Wyk de Vries & Borgia 1996) to identify nondimensional groupings that delimit regions of stable and unstable volcano growth.

Here, we treat the problem through an analytical formulation.

Settling Time for a Volcano Spreading on a Viscous Substrate

A simple model for spreading embodies a rigid basement, followed upward by a ductile and a brittle layer overlain, in turn, by the volcanic edifice (Figure 12). The evolution of the boundary $h(x, t)$ between these layers evolves from the differential pressure imposed by the load of the volcano on the substratum. The viscous layer flows from the volcanic center toward the periphery while the rigid basement and the brittle layer resist this flow, building elastic stresses. Stresses within the brittle layer are extensional at the volcanic center and compressional around the periphery. Ultimately, the elastic stresses may overcome the fracture resistance of the brittle substratum, which fails by forming thrust faults at the volcanic periphery and grabens at the center.

The volcano has density ρ_v, thickness H_v, and half-width L_v. The brittle substratum has density ρ_b, thickness H_b, and half-distance between the peripheral thrusts L_b. The ductile substratum of initial thickness H_d is assumed to be incompressible, Newtonian, and with constant viscosity μ_d and density ρ_d. If the thickness of the ductile substratum is much less than the half-distance between the peripheral thrusts of the brittle substratum ($H_d/L_b << 1$), we can apply the lubrication approximation of the Navier-Stokes equations, valid for low Reynolds numbers:

$$\begin{cases} \dfrac{\partial v_x}{\partial x} + \dfrac{\partial v_z}{\partial z} = 0 & \text{mass conservation} \quad (1a) \\ -\dfrac{\partial p}{\partial x} + \mu_d \dfrac{\partial^2 v_x}{\partial z^2} = 0 & x\text{-momentum conservation} \quad (1b) \\ -\dfrac{\partial p}{\partial z} - \rho_d g = 0 & z\text{-momentum conservation} \quad (1c) \end{cases}$$

where v_x and v_z are, respectively, the velocities of ductile substratum in the horizontal x and vertical z directions, p is the distribution of pressure within ductile substratum, and g is the gravity acceleration.

The boundary conditions for the governing equations are:

$$v_z|_{z=h} = \int_{v_z|_{z=0}}^{v_z|_{z=h}} \partial v_z = \frac{\partial h}{\partial t} \quad (2a1)$$

$$v_z|_{z=0} = 0 \quad (2a2)$$

$$v_x|_{z=0} = 0 \quad (2b1)$$

$$v_x|_{z=h} = 0 \left[\text{or } \left.\frac{\partial v_x}{\partial z}\right|_{z=h} = -\frac{\tau_d(x)}{\mu_d} \right] \quad (2b2)$$

$$p|_{z=h} = P_d(x, t). \quad (2c)$$

The second alternative boundary condition in Equation 2b2 becomes appropriate once the brittle substratum fails under the load of the volcano and begins to extend. In this equation $\tau_d(x)$ is the local shear stress applied to the ductile layer by the deforming brittle layer. $P_d(x, t)$ in Equation 2c is a function of the shape of the volcano and assumes that the angle of internal friction of the volcano and the brittle layer have no influence on the deformation of the substratum. Where Equations 1*a,b,c* are quasi-steady, the time dependence of spreading enters through the free-surface kinematic boundary condition, Equation 2a1.

Integrating Equations 1*a,b,c* under the above conditions and combining leads to:

$$\frac{\partial h}{\partial t} = \frac{1}{3c\mu} \frac{\partial}{\partial x} \left(h^3 \frac{\partial p}{\partial x} \right), \quad (3)$$

where $c = 4$ for the first boundary condition of no deformation in the brittle layer in Equation 2b2, and $c = 1$ for the second condition of no shear stress applied by the brittle layer. We approximate $p(x, t)$ as a hydrostatic pressure distribution on the substratum:

$$p(x) = P_{atm} + \rho_v i_v + \rho_b g H_b + \rho_d g(h - z), \quad (4)$$

where P_{atm} is the atmospheric pressure and $h_v = h_v(x, t)$ is the shape of the volcano. Evaluating $\partial p/\partial x$ from Equation 4 and substituting it in Equation 3, we obtain:

$$\frac{\partial h}{\partial t} = \frac{g}{3c\mu}\frac{\partial}{\partial x}\left(h^3\frac{\partial}{\partial x}(\rho_d h + \rho_v h_v)\right). \quad (5)$$

The initial and boundary conditions for Equation 5 are then:

$$h|_{t=0} = H_d \quad (6a)$$

$$\left.\frac{\partial h}{\partial x}\right|_{x=\infty} = 0 \quad (6b)$$

$$h|_{x=\infty} = H_d. \quad (6c)$$

The initial condition, Equation 6a, states that the thickness of ductile substratum at the initial time is constant. The boundary conditions, Equations 6b and 6c, states that the ductile and brittle layers remain undisturbed at distances far from the volcano.

To make Equations 6 dimensionless, we scale using the pressure because the ductile layer of the substratum is usually much thinner than the height of the volcano, $H_d/H_v \leq 1$, so that

$$\xi = \frac{x}{L_v} \quad (7a)$$

$$\eta = \frac{h}{H_d} \quad (7b)$$

$$\eta_v = \frac{h_v}{H_v} \quad (7c)$$

$$\tau = \frac{t}{T}, \quad (7d)$$

where T is the characteristic time for deformation of the viscous substrate, a quantity of great interest for all volcanoes that spread. We then obtain:

$$\frac{3c\mu}{T\rho_v g H_v}\left(\frac{L_v}{H_d}\right)^2\frac{\partial\eta}{\partial\tau} = \frac{\partial}{\partial\xi}\left\{\eta^3\frac{\partial}{\partial\xi}\left[\left(\frac{\rho_d H_d}{\rho_v H_v}\right)\eta + \eta_v\right]\right\}, \quad (8)$$

which is the general expression for the evolution of the deforming viscous substrate. A similar equation is easily derived for cylindrical coordinates with the same nondimensional groupings.

For time dependence of the spreading to be important, the dimensionless grouping in the left-hand side of Equation 8 is of order unity, and so:

$$T = \left(\frac{L_v}{H_d}\right)\frac{3c\mu}{\rho_v g H_v}. \quad (9)$$

If the parameters on the right-hand side of Equation 9 were known, the estimate of characteristic spreading time T thus obtained could be compared with the age

or duration since the last major growth phase of a volcano to predict the stage of spreading. In practice, viscosity is poorly known, so we suggest that the growth time, or age, of spreading volcanoes may be substituted for T and used with the other parameters to estimate substrate viscosities.

Because T is defined by Equation 9, the dimensionless grouping in the left-hand side of Equation 8 becomes unity. Then Equation 8 can have two cases. First, if the thickness of the ductile layer is comparable to the height of the volcano, $\rho_d H_d/\rho_v H_v = O(1)$, as at Concepciòn, for instance, then

$$\frac{\partial \eta}{\partial \tau} = \frac{\partial}{\partial \xi}\left\{\eta^3 \frac{\partial}{\partial \xi}\left[\left(\frac{\rho_d H_d}{\rho_v H_v}\right)\eta + \eta_v\right]\right\}, \tag{10}$$

which is a diffusion-like equation. As the steady state is approached, then we find

$$\eta = \frac{\rho_v H_v}{\rho_d H_d} - \eta_v, \tag{11}$$

which is the application of Archimedes' principle. Second, if the thickness of the ductile layer is small in comparison to the height of the volcano, $\rho_d H_d/\rho_v H_v << 1$, as at Kilauea, then

$$\frac{\partial \eta}{\partial \tau} = \frac{\partial}{\partial \xi}\left[\eta^3 \frac{\partial \eta_v}{\partial \xi}\right]. \tag{12}$$

This is a rather simple equation because the second derivative on the right-hand side is the known slope of the volcano.

Morphologic and Structural Radii of Spreading Volcanoes

In the derivation of the preceding we have assumed that the radius of a volcano L_v is a quantity that can be defined unambiguously. Although it would seem that all volcanoes possess what we would hope to be this radius, it is difficult or practically impossible to determine because of irregularities in the tapering of distal deposits. What we call the morphological and structural radii of spreading volcanoes, however, can be precisely defined and measured, as we now show. We first note that any volcanic shape function yields a characteristic radius. Consider, for instance, the exponential shape:

$$h_v = H_v e^{-x/L_e} \text{ or } \eta_v = e^{-L_v/L_e \xi}, \tag{13}$$

in dimensional and nondimensional forms, where L_e is what we call the geometric radius, a parameter fitted to the actual shape of a volcano. This radial distance occurs where a volcano's height is $H_v\, e^{-1}$, a little more than one third of H_v. This distance, or any like it, exists independently of considerations of geologic processes.

Volcanoes that spread over a relatively thick ductile layer produce a morphologic radius L_m based on the extent of sinking into that layer. Sinking is limited by the thickness of the ductile layer (that is, its thickness cannot be less than

zero). Recalling Equation 11 for volcanoes such as Concepciòn, it follows that for $H_d < H_v$ the value of the radial distance for which $\eta = 0$ is the distance at which the brittle substratum touches the bottom of the ductile layer. In practice, this forms at the surface a break in volcanic slope. Thus, for the condition given by the exponential shape function, Equation 13, we have

$$L_m = -L_e \ln\left(\frac{\rho_v H_v}{\rho_d H_d}\right). \quad (14)$$

This morphologic radius L_m is a direct function of the geometric radius L_e and the thickness of the substratum. More generally, the morphological radius changes with time and does not require a volcano to sink entirely through its ductile substrate.

To calculate the structural radius of a spreading volcano, we determine the distance for emergence of thrust faults from beneath their peripheries. The shear stress that deforms the viscous layer is transmitted to the brittle layer which stores stresses elastically. If this elastic stress exceeds the critical stress for failure, the layer fails, forming thrust faults. Integrating Equations 1 with the boundary conditions, Equations 2, for spreading at incipient failure of the brittle layer, we obtain the shear stress at the base of the brittle layer $z = h$

$$\tau_{xz}|_{z=h} = -\frac{\rho_v g}{2} h \frac{\partial}{\partial x}\left(\frac{\rho_d}{\rho_v} h + h_v\right). \quad (15)$$

The horizontal stress σ_x along the brittle layer due to flow in the ductile layer σ_x may be approximated by integrating the shear stress at its base, Equation 15, with respect to x to obtain the force per unit width. Dividing by thickness of the brittle layer H_b we obtain

$$\sigma_x = \frac{1}{H_b} \int |\tau_{xz}|_{z=h}| \partial x. \quad (16)$$

Substituting Equation 15 and solving this integral, we obtain our approximation

$$\sigma_x = \frac{\rho_v g H_v}{2H_b}\left[h\left(1 - \frac{h_v}{H_v}\right) - \frac{\rho_d}{2\rho_v}\left(\frac{h^2 - h_0^2}{H_v}\right)\right], \quad (17)$$

where we have used the following boundary condition:

$$h|_{x=0} = h_0,\ h_v|_{x=0} = H_v \text{ and } \sigma_x|_{x=0} = 0. \quad (18)$$

The horizontal stress in the brittle layer is maximum, therefore, where the thickness of the volcano is zero. Finally, σ_x must be balanced by the elastic stress within the brittle layer and σ_z, which is approximated by the weight

$$\sigma_z = g[\rho_v h_v + \rho_b H_b]. \quad (19)$$

We now have expressions for the horizontal and vertical stresses within the brittle layer.

It is now of interest to calculate the normal σ and shear τ tractions on the eventual failure planes within the brittle layer assuming a Coulomb fracture criterion $\tau = \sigma \tan \phi$ with insignificant cohesion, ϕ being the angle of internal friction. With this criterion, σ_x and σ_z are related to ϕ through:

$$\left.\frac{\sigma_x}{\sigma_z}\right|_{x=L_t} = N_\phi = \frac{1 + \sin\phi}{1 - \sin\phi} \tag{20}$$

because σ_x and σ_z become the maximum and minimum stresses, respectively, of the base of the volcano. For any reasonable value of the angle of internal friction of the brittle layer, $20° < \phi < 40°$, N_ϕ ranges from 2.0 to 4.6.

Substituting Equations 17 and 19 into Equation 20 and rearranging, we have

$$\frac{h_v}{H_v} = \frac{1 - 2N_\phi \frac{H_b}{h}\frac{H_b}{H_v}\frac{\rho_b}{\rho_v} - \frac{1}{2}\frac{\rho_d}{\rho_v}\left(\frac{h^2 - h_0^2}{hH_v}\right)}{1 + 2N_\phi \frac{H_b}{h}}. \tag{21}$$

Equation 21 can be rearranged with $h = h_0 = H_d$, the beginning of the deformation, and the volcanic-shape function, Equation 13, to yield the structural radius

$$L_t = -L_e \ln\left(\frac{1 - 2N_\phi \frac{H_b}{H_d}\frac{H_b}{H_v}\frac{\rho_b}{\rho_v}}{1 + 2N_\phi \frac{H_b}{H_d}}\right), \tag{22}$$

which has real solutions for

$$2N_\phi \frac{H_b}{H_d}\frac{H_b}{H_v}\frac{\rho_b}{\rho_v} < 1. \tag{23}$$

This solution, developed in rectangular coordinates, applies equally in cylindrical coordinates because the failure zone is far from the volcanic center. If the ratio of the densities is of order unity, then we have

$$H_b < n\sqrt{H_d H_v}, \tag{24}$$

where n is about 0.5, 0.4, and 0.3 for ϕ equal to 20°, 30°, and 40°, respectively. Thrust faulting at the bases of volcanoes occurs when H_b, the thickness of the brittle layer, is smaller than a critical value that can be calculated from simple geologic data, the angle of internal friction of the brittle substratum ϕ, the thickness of the ductile layer H_d, and the height of the volcano H_v.

Finally, then, the structural radius L_t of a spreading volcano, being the maximum distance of propagation of deformation, probably corresponds best to the scaling radius L_v (Figure 11), which is retrospectively identified on a physical rather than lithologic or geometric basis.

Scaling Analysis

Merle & Borgia (1996) used the Buckingham-Π theorem to scale laboratory experiments to volcanoes spreading on a viscous substratum. The experiments were used to obtain critical values of the spreading process. Using the variables described in the previous section, we have 12 variables and 3 dimensions (space, mass, and time). Therefore, according to the theorem, there must be 9 independent dimensionless groupings (Table 1), which characterize the system. The first groupings are the five geometric ratios of the system:

$$\frac{H_v}{L_v} = \frac{\textit{height of volcano}}{\textit{radius of volcano}} = \text{potential instability} \qquad (25a)$$

$$\frac{H_b}{L_v} = \frac{\textit{thickness of brittle substratum}}{\textit{radius of volcano}} = \text{substratum strength} \qquad (25b)$$

TABLE 1 Relations between dimensionless numbers

Name	Definition	Merle & Borgia (1996)
Potential instability	$\frac{H_v}{L_v} = \frac{\textit{height of volcano}}{\textit{radius of volcano}}$	Π_1
Strength of subs.	$\frac{H_b}{L_v} = \frac{\textit{thickness of brittle substratum}}{\textit{radius of volcano}}$	$\Pi_1 * \pi_2$
Weakness of subs.	$\frac{H_d}{L_v} = \frac{\textit{thickness of ductile substratum}}{\textit{radius of volcano}}$	$\frac{\Pi_1 * \pi_2}{\Pi_3}$
Scaled volcanic radius	$\frac{L_v}{L_e} = \frac{\textit{radius of volcano}}{\textit{geometric radius of volcano}}$	—
Scaled thrusting distance	$\frac{L_t}{L_e} = \frac{\textit{radius to thrust faulting}}{\textit{geometric radius of volcano}}$	—
Volcano floating potenital	$\frac{\rho_d H_d}{\rho_v H_v} = \frac{\textit{pressue of ductile substratum}}{\textit{pressure of volcano}}$	$\frac{\Pi_2}{\Pi_3 * \Pi_4}$
Brit. subs floating potential	$\frac{\rho_d H_d}{\rho_b H_b} = \frac{\textit{pressure of ductile substratum}}{\textit{pressure of brittle substratum}}$	—
Process restraint	$2N_\phi \frac{H_b}{H_d}\frac{H_b}{H_v}\frac{\rho_b}{\rho_v} = \frac{\textit{failure resistance force}}{\textit{failure inducing force}}$	defined differently grm Π_6
Process rate	$\frac{3c\mu}{\rho_v g H_v T}\left(\frac{L_v}{H_d}\right)^2 = \frac{\textit{viscous force}}{\textit{gravitational force}}$	$\frac{3c}{\Pi_1^2 * \Pi_5}$
Reynolds number	—	Π^7

$$\frac{H_d}{L_v} = \frac{\textit{thickness of ductile substratum}}{\textit{radius of volcano}} << 1 = \text{substratum weakness} \quad (25c)$$

$$\frac{L_v}{L_e} = \frac{\textit{radius of volcano}}{\textit{geometric radius of volcano}} = \text{scaled volcanic radius} \quad (25d)$$

$$\frac{L_t}{L_e} = \frac{\textit{structural radius of volcano}}{\textit{geometric radius of volcano}} = \text{scaled thrusting distance} \quad (25e)$$

Equation 25c is the ratio used for deriving the lubrication approximation (Equations 1) of the Navier-Stokes equations. If the structural radius is taken as the radius of the volcano, as suggested in the previous section, Equations 25d and 25e become identical. Another two groupings depend on the densities of the ductile layer, brittle layer, and volcano and are used in simplifying Equation 8:

$$\frac{\rho_d H_d}{\rho_v H_v} = \frac{\textit{pressure of ductile substratum}}{\textit{pressure of volcano}} = \text{volcano float potential} \quad (25f)$$

$$\frac{\rho_d H_d}{\rho_b H_b} = \frac{\textit{pressure of ductile substratum}}{\textit{pressure of brittle substratum}} = \text{brittle substratum float potential} \quad (25g)$$

The final two numbers must be ratios of the forces per unit volume acting on the system. These are the resistance to failure of the brittle substratum, the gravity, and the viscous force in the ductile substrate. The inertial force is insignificant relative to the other forces, as a consequence of the lubrication approximation (Equation 1). From Equation 23, we have:

$$2N_\phi \frac{H_b}{H_d}\frac{H_b}{H_v}\frac{\rho_b}{\rho_v} = \frac{\textit{failure resistance force}}{\textit{failure inducing force}} = \text{process restraint} \quad (25h)$$

and from Equation 8,

$$\frac{3c\mu}{\rho_v g H_v T}\left(\frac{L_v}{H_d}\right)^2 = \frac{\textit{viscous force}}{\textit{gravitational force}} = \text{process rate}, \quad (25i)$$

where this last grouping encapsulates the rate of deformation.

A comparison of the dimensionless groupings derived here from first principles with those obtained by Merle & Borgia (1996) using the Buckingham-Π theorem leads to the relations between them (Table 1). Most of these groupings are the product combinations of the Π's of Merle & Borgia (1996). A few differences arise between their formulation and ours. Equations 25d and 25e were not considered by Merle & Borgia (1996) because the parameters L_e and L_t were not used. Also, Equation 25g is not present in Merle & Borgia (1996) because the experimental volcano had the same density as that of the brittle substratum. In addition, they use a different definition of the process restraint grouping, Equation 25h, corresponding to Π_6, and use the Reynolds number, which is insignificant in the lubrication approximation used here. The range of values of the dimen-

sionless numbers for real and experimental volcanoes are listed in Table 2. From a similarity argument, the numbers derived by Merle & Borgia (1996) using the Buckingham-Π theorem are perfectly acceptable, though this theorem gives no clue for formulating the parameters. Our derivation, starting from first principles, finds physically significant forms of the dimensionless parameters.

An example of the relevance of the above statement may be taken from the critical values for spreading as calculated by Merle & Borgia (1996). These authors found that in experiments with no significant density contrast between volcano and substratum and with $\phi = 30°$, spreading occurs if the following two conditions are verified:

$$\Pi_2 = \frac{H_b}{H_v} < 0.3 \pm 0.1 \tag{26a}$$

$$\Pi_3 = \frac{H_b}{H_d} < 2 \pm 1. \tag{26b}$$

These conditions are equivalent to the one expressed in Equation 23. In fact, for the experimental set up of Merle & Borgia (1996), Equation 23 may be written as

$$\frac{H_b^2}{H_d H_v} = \pi_2 \pi_3 < 0.17. \tag{27a}$$

The value of the theoretically determined equation 27 is consistent with the experimentally determined values of π_2 and π_3, $0.6 \pm 0.5 \simeq 0.17$. Thus, Equation 24 is a definition of the spreading limit criteria based on physical grounds and verified within experimental errors.

TABLE 2 Average values of the dimensionless parameters

Merle & Borgia	Field min	max	Experients init	final	Borgia, Delaney & Denlinger
π_1	0.24	0.15	0.59	0.18	Potential instability
π_2	0.00	0.33	0.10	0.22	Intrinsic strength of sub
π_3	0.00	1.00	1.00	2.00	Intrinsic weakness of sub
					Relative volcanic radius
					Relative thrusting distance
π_4	1.25	1.40	1.00	1.00	Volcano floating potent
					Brittle substr. float. potent
π_5	29.40	82.32	1200.50	552.23	Process rate
π_6	5.52	51.94	508.86	259.34	Process restrain
π_7	2.00E-19	2.00E-21	5.00E-11	1.25E-11	Reynolds number

DISCUSSION

We presented examples of volcanoes dissected and underlain by faults. We also demonstrated that volcanoes built upon relatively weak substrates are subject to spreading motions caused by faulting and flow in response to the horizontal pressure gradients exerted by the weight of volcanic overburden. These structures exist on many volcanoes, though they are more common on larger constructs. Their structural expression is often subtle, both because younger volcanic deposits tend to obliterate them and because many of the most important structures are exposed along or beyond volcanic peripheries, where volcanologists tend to underestimate their importance. We note that many volcanoes lack spreading structures of the type we have emphasized. Among these, many are subject to the sector collapses that produce debris avalanches, which are now well recognized by their distinctive morphology.

Landslides and Sector Collapses

Sector collapses represent a particular type of rapid asymmetric spreading or landsliding. The danger of these collapses was indelibly imprinted in the minds of volcanologists by the 1980 collapse and lateral blast at Mount St. Helens (Lipman & Mullineaux 1981). Considerable speculation persists as to whether the sector collapse at Mount St. Helens triggered the eruption or vice versa. Indeed, considerable slumping of the north flank of Mount St. Helens, which averaged about 2 m/day, was commingled with intermittent precursory eruptions, mainly of phreatic origin, during the several months before the culminating slope failure and Plinian eruption. Importantly, the collapse followed by about ten seconds (Voight 1981) a shallow earthquake of magnitude 5.1, the largest measured during the Mount St. Helens eruptive sequence.

Following the Mount St. Helens crisis, recognition of horseshoe-shaped craters at other volcanic summits led to the realization that large collapses are common to many of the world's volcanoes (see Francis & Self 1987, Siebert 1992). Many sector-collapse amphitheaters have been refilled by subsequent dome building as well as ponding and overflow of eruptive products. In such instances, collapses are identified by hummocky deposits of volcanic avalanche debris. Interestingly, while the addition of new magma clearly helped to destabilize the north flank of Mount St. Helens, this needn't always be the case, as seen at Bandaisan volcano in Japan during its collapse in 1888. The record seems to underscore the importance of nearby earthquakes in triggering volcanic landsliding and collapse.

Finally, as seems to be the case at Piton de la Fournaise (discussed earlier), volcanic spreading and catastrophic collapse can be closely related (see Van Wyk de Vries & Francis 1987).

Dike Intrusion and Flank Instability

It has been long argued that dilation of dikes, especially along volcanic rift zones, compresses and thus destabilizes adjacent volcanic flanks. Perhaps the most complete treatment of this process was done by Elsworth & Voight (1995, 1996) and

Voight & Elsworth (1997). These workers recognized that stress changes induced by intrusion decay rather strongly as a function of distance from the dike. Therefore, they went on to test the hypothesis that mechanical and thermal pressurization of groundwater is capable of decreasing the effective strength of fault surfaces, which are then more susceptible to mechanical instability. Indeed, relations between dike intrusion and subsequent seismic activity during 1949 at Cumbre Vieja, Canary Islands and during 1951 and 1995 at Fogo, Cape Verde Islands seem consistent with delays associated with diffusion of groundwater as it escapes regions of pore-volume collapse and heating near dike walls (Elsworth & Day 1999).

Other workers, however, have suggested that additional processes must be at play. At Kilauea, dike intrusions are typically only several kilometers high and are much closer to the surface than the 8–9-km focal depths of the larger flank earthquakes. Accordingly, analysis of flank stability there postulates the presence of magma throughout the entire height of the edifice (Dieterich 1988, Iverson 1995). For the most part, these analyses of slope stability require pore-fluid pressures near the decollement that approach lithostatic values. The reason for this is not difficult to understand: For the 70-km-wide flank of Kilauea to slide seaward because of a load applied from the 9-km-high rift system, the basal decollement must behave in a very slippery fashion. If the basal decollement exhibited high friction, then increased rift-zone loading would eventually produce faulting to the surface over a horizontal length comparable to the loading depth of 9 km. This difficulty is overcome by supposing the flank has bulk viscosities in the range of 10^{18} to 10^{20} Pa·s (Borgia 1994), in which case spreading of the flank produces a shape and structures much like those observed at Hawaiian volcanoes.

Lava Domes and Venusian Volcanoes

Several recent volumes (see Fink 1987, 1990) provide a broad survey of lava-dome structure and emplacement processes, which encompasses a certain kind of volcanic spreading by viscous flow of magmas under the influence of their own weight. Theoretical treatments of dome growth successfully predict relations between height and radius (Blake 1990, Fink & Griffiths 1998, Griffiths 1999), as well as cross-sectional profiles and temporal evolution, based on magma viscosity and yield strength. Nonetheless, lava-dome growth is confined to individual eruption sequences, and spreading motion does not directly affect, for instance, the structural evolution of the composite volcano upon which the dome may sit. Alternatively, lava domes may be viewed as high-viscosity lava flows that happen to be axisymmetric (Griffiths 1999) or flows held within brittle, solidified carapaces that resist the lava pressure (Iverson 1990).

Some volcanoes on Venus seem to resemble lava domes—their ''pancake'' shapes are attributable to the very high atmospheric pressure of that planet and to the low yield strength of the probable basaltic or andesitic magmas (Head 1996, Fink & Griffiths 1998). These volcanoes are large (most range from 10 to 60 km

in diameter), but not particularly high; most measured to date stand less than 1,500 m above their surroundings (Pavri et al 1992). Although the volumes of these volcanoes range up to about 3,000 km^3, they appear to have been emplaced in single eruptions. Most of the pancake volcanoes possess fracture systems of lengths that greatly exceed the heights of the volcanoes. Therefore, these fracture systems are likely to cut entirely through the volcanoes. Additionally, many of these volcanoes are associated with coronae, circumferential fractures that surround their peripheries. Taken together, both types of fractures indicate brittle deformation of the same general age as the volcanism. Head (1996) suggests that the thickness of crust above the magma reservoirs feeding these flows is rather thin, so that co-eruptive subsidence caused by reservoir deflation has a profound affect on ground surface deformation.

The pancake volcanoes of Venus represent less than 10% of the total number identified there by Magellan data. Although volcanic fields on Venus range up to 800 km in diameter, most shield volcanoes are less than 100 km in diameter and stand less than 2 km high (Head et al 1992, Head 1996). While their low height-to-diameter ratio serves to inhibit spreading of the edifice, many of these enormous volcanoes are sited in coronae that are indicative of deformation of the substrate. The coronae, however, are thought to result from ground-surface faulting caused by co-eruptive draining of shallow magma reservoirs underlying the volcanoes. Slope failures have been identified on many Venusian volcanoes (Bulmer & Guest 1996) and are a result of both explosive eruptions and oversteepening of edifices.

CONCLUSIONS

We have examined processes by which volcanic edifices spread horizontally under the influence of their own weight and of loads applied by magma reservoirs in or just beneath these edifices. Although it has been well established for almost two decades that volcanoes collapse by transporting debris down their slopes during catastrophic landslides and sector collapses, it is only now becoming clear that a broader set of spreading processes affects the structural evolution of most large volcanoes. These processes include radial flow of volcanic substrates from beneath volcanic constructs (in at least one instance, we document the diapiric rise of such material into and through the constructs); decollement faulting at the base of volcanic edifices; and, of course, faulting within the edifice itself. These motions leave behind, as records of the spreading process, the scarps exposed on volcanic slopes, many of which extend to form polyhedral as well as concentric patterns. They also leave behind thrust faults exposed at the volcanic periphery or even some distance beyond. Volcanic rift zones and transform-fault structures are also indicators of spreading.

Examination of these physical processes has been pursued through several lines of attack. Some spreading volcanoes can be viewed as Coulomb wedges

that adjust their slopes so as to remain in a state of incipient instability. They may also be viewed as slopes constantly susceptible to landslides. Finally (and this view is the least understood), they may be viewed as loads placed upon weak substrates forced as a result to flow horizontally out from beneath. We estimated the time required for this horizontal flow and the distance from the volcanic center for emergence of thrust faults above the weak substrates. In all cases, deformations work to extend the volcano horizontally as its summit regions subside. While many of these motions are secular, others are catastrophic. Thus, volcanic spreading ranges from mechanisms that may include rock creep to mechanisms encompassing large-magnitude earthquakes and large-runout landslides.

LITERATURE CITED

Blake S. 1990. Viscoplastic model of lava domes. In *Lava Flows and Domes*, ed. JH Fink. *IAVCEI Proc. Volcanology* 2:88–128

Borgia A. 1994. Dynamic basis of volcanic spreading. *J. Geophys. Res.* 99:17791–804

Borgia A, Burr J, Montero W, Morales LD, Alvarado GE. 1990. Fault propagation folds induced by gravitational failure and slumping of the central Costa Rica volcanic range: implications for large terrestrial and Martian volcanic edifices. *J. Geophys. Res.* 95:14357–82

Borgia A, Ferrari L, Pasquaré G. 1992. Importance of gravitational spreading in the tectonic and volcanic evolution of Mount Etna. *Nature* 357:231–35

Borgia A, Lanari R, Sansosti E, Tesauro M, Berardino P, et al. 2000. Actively growing anticlines beneath Catania form the distal motion of Mount Etna's decollement measured by SAR interferometry and GPS. *Geophys. Res. Lett.* Submitted

Borgia A, Treves B. 1992. Volcanic plates overriding the ocean crust: structure and dynamics of Hawaiian volcanoes. In *Ophiolites and Their Modern Oceanic Analogues*, ed. WJ McGuire, AP Jones, J Neuberg. *Geol. Soc. Sp. Publ.* 60:277–99

Bulmer MH, Guest JE. 1996. Modified volcanic domes and associated debris aprons on Venus. See McGuire et al 1996, pp. 349–72

Calvari S, Tanner LH, Gropelli G. 1998. Debris-avalanche deposits of the Milo Lahar sequence and the opening of the Valle del Bove on Etna volcano (Italy). *J. Volcanol. Geotherm. Res.* 87:193–209

Clague DA. 1995. Petrology of submarine lavas from Kilauea's Puna Ridge, Hawaii. *J. Petrol.* 36:299–349

Clague DA, Denlinger RP. 1994. Role of olivine cumulates in destabilizing the flanks of Hawaiian volcanoes. *Bull. Volc.* 56:425–34

Crumpler LS, Head JW, Aubele JC. 1996. Calderas on Mars: characteristics, structure, and associated flank deformation. See McGuire et al 1996, pp. 307–48

Delaney PT, Denlinger RP. 2000. Stabilization of volcanic flanks by dike intrusion. *Bull. Volc.* 61:356–62

Delaney PT, Denlinger RP, Lisowski M, Miklius A, Okubo PG, et al. 1998. Volcanic spreading at Kilauea, 1976–1996. *J. Geophys. Res.* 103:18003–23

Delaney PT, Fiske RS, Miklius A, Okamura AT, Sako MK. 1990. Deep magma body beneath the summit and rift zones of Kilauea volcano, Hawaii. *Science* 247: 1311–16

Delaney PT, Miklius A, Arnadottir T, Okamua AT, Sako MK. 1993. Motion of Kilauea Volcano during sustained eruption from the Pu'u O'o and Kupaianaha vents, 1983–1991. *J. Geophys. Res.* 98:17801–20

Denlinger RP, Okubo P. 1995. Structure of the mobile south flank of Kilauea Volcano, Hawaii. *J. Geophys. Res.* 100:24499–507

De Voogd B, Pou Palomé S, Hirn A, Charvis P, Gallart J, et al. 1999. Vertical movements and material transport during hotspot activity: seismic reflection profiling offshore La Réunion. *J. Geophys. Res.* 104:2855–74

Dieterich JH. 1988. Growth and persistence of Hawaiian volcanic rift zones. *J. Geophys. Res.* 93:4258–70

Elsworth D, ed. 2000. Deformation and flank instability of oceanic island volcanoes: a comparison of Hawaii with Atlantic island volcanoes. *J. Volc. Geotherm. Res.* In press

Elsworth D, Day SJ. 2000. Flank collapse triggered by intrusion: the Canarian and Cape Verde archipelagoes. *J. Volc. Geotherm. Res.* In press

Elsworth D, Voight B. 1995. Dike intrusion as a trigger for large earthquakes and the failure of volcano flanks. *J. Geophys. Res.* 100:6005–24

Elsworth D, Voight B. 1996. Evaluation of volcano flank instability triggered by dyke intrusion. See McGuire et al 1996, pp. 45–53

Evamy BD, Haremboure J, Kamerling P, Knaap WA, Molloy FA, Rowlands PH. 1978. Hydrocarbon habitat of Tertiary Niger Delta. *Am. Assoc. Petrol. Geol. Bull.* 62:1–39

Fink JH, ed. 1987. *The Emplacement of Silicic Domes and Lava Flows. Geol. Soc. Am. Sp. Pap. 212*

Fink JH, ed. 1990. *Lava Flows and Domes. IAVCEI Proc. Volc.* 2. Berlin: Springer-Verlag. 249 pp.

Fink JH, Griffith RW. 1998. Morphology, eruption rates, and rheology of lava domes: insights from laboratory models. *J. Geophys. Res.* 103:527–45

Firth C, Stewart I, McGuire WJ, Kershaw S, VitaFinzi C. 1996. Coastal elevation changes in eastern Sicily: implications for volcano instability at Mt. Etna. See McGuire et al 1996, pp. 153–67

Francis P, Self S. 1987. Collapsing volcanoes. *Sci. Am.* 256:90–97

Griffiths RW. 1999. The dynamics of lava flows. *Annu. Rev. Fluid Mech.* 32:477–518

Guest JE, Chester DK, Duncan AM. 1984. The Valle del Bove, Mount Etna: its origin and relation to the stratigraphy and structure of the volcano. *J. Volc. Geotherm. Res.* 21:1–23

Head JW. 1996. Volcano instability development: a planetary perspective. See McGuire et al 1996, p. 2544

Head JW, Crumpler LS, Aubele JC, Guest JE, Saunders RS. 1992. Venus volcanism: classification of volcanic features and structures, associations, and global distribution from Magellan data. *J. Geophys. Res.* 97:13153–97

Iverson RM. 1995. Can magma injection and groundwater forces cause massive landslides on Hawaiian volcanoes? *J. Volc. Geotherm. Res.* 66:295–308

Iverson RM. 1990. Lava domes modeled as brittle shells that enclose pressurized magma, with application to Mount St. Helens. In *Lava Flows and Domes: Emplacement Mechanisms and Hazard Implications,* ed. JH Fink. *IAVCEI Proc. Volcanology* 2:47–69

Jackson JA, ed. 1997. *Glossary of Geology.* Alexandria, VA: Am. Geol. Inst. 769 pp.

Labazuy P. 1996. Recurrent landslides events on the submarine flank of Piton de la Fournaise volcano (Reunion Island). See McGuire et al 1996, pp. 295–306

Lanari R, Lundgren P, Sansosti E. 1998. Dynamic deformation of Etna volcano observed by satellite radar interferometry. *Geophys. Res. Lett.* 25:1541–44

Lipman PW, Lockwood JP, Okamura RT, Swanson DA, Yamashita KM. 1985. *Ground deformation associated with the 1975 magnitude 7.2 earthquake and resulting changes in activity of Kilauea volcano, Hawaii. U.S. Geol. Surv. Prof. Pap.* 1276

Lipman PW, Mullineaux DR, eds. 1981. *The 1980 Eruptions of Mount St. Helens, Washington. U.S. Geol. Surv. Prof. Pap. 1250*

Lundin ER. 1989. Thrusting of the Clarion Formation, the Bryce Canon region, Utah. *Geol. Soc. Am. Bull.* 101:1038–50

McGuire WJ, Jones AP, Neuberg J, eds. 1996. *Volcano Instability on the Earth and Other Planets. Geol. Soc. Sp. Pub.* 110, 388 pp.

Merle O, Borgia A. 1996. Scaled experiments of volcanic spreading. *J. Geophys. Res.* 101:13,805–817

Merle OR, Davis GH, Nickelsen RP, Gourlay PA. 1993. Relation of thin-skinned thrusting of Colorado Plateau strata in southwestern Utah to Cenozoic magmatism. *Geol. Soc. Am. Bull.* 105:387–98

Merle OR, Vendeville B. 1995. Experimental modelling of thin-skinned shortening around magmatic intrusions. *Bull. Volc.* 57:33–43

Montalto S, Vinciguerra S, Menza S, Patane G. 1996. Recent seismicity of Mount Etna: implications for flank instability. See McGuire et al 1996, pp. 169–77

Moore JG, Normark WR, Holcomb RT. 1994. Giant Hawaiian landslides. *Annu. Rev. Earth Planet. Sci.* 22:119–44

Owen S, Segall P, Freymueller J, Miklius A, Denlinger R, et al. 1995. Rapid deformation of the south flank of Kilauea volcano, Hawaii. *Science* 267:1328–32

Owen S, Segall P, Lisowski M, Miklius A, Denlinger RP, Sako M. 2000. The rapid deformation of Kilauea volcano: GPS measurements between 1990 and 1996. *J. Geophys. Res.* Submitted

Pavri B, Head JW, Klose KB, Wilson L. 1992. Steep-sided domes on Venus: characteristics, geologic setting, and eruption conditions from Magellan data. *J. Geophys. Res.* 97:13445–78

Prosser JT, Carr MJ. 1987. Poás volcano, Costa Rica: geology of the summit region and spatial and temporal variations among the most recent lavas. *J. Volc. Geotherm. Res.* 33:131–46

Rasà R, Azzaro R, Leonardi O. 1996. Aseismic creep on faults and flank instability at Mount Etna, Sicily. See McGuire et al 1996, pp. 179–92

Rust D, Neri M. 1996. The boundary of large-scale collapse on the flank of Mt. Etna, Sicily. See McGuire et al 1996, pp. 193–208

Siebert L. 1992. Threats from debris avalanches. *Nature* 356:658–59

Smith JR, Malahoff A, Shor AN. 2000. Submarine geology of the Hilina slump and morphostructural evolution of Kilauea volcano, Hawaii. *J. Volc. Geotherm. Res.* In press

Thomas PJ, Squyres SW, Carr MH. 1990. Flank tectonics of Martian volcanoes. *J. Geophys. Res.* 95:14345–56

Van Bemmelen RW. 1949. *The Geology of Indonesia. General Geology of Indonesia and Adjacent Archipelagos* 1A. The Hague, The Netherlands: Government Printing Office. 732 pp.

Van Wyk de Vries B, Borgia A. 1996. The role of basement in volcano deformation. See McGuire et al 1996, pp. 95–110

Van Wyk de Vries B, Francis PW. 1997. Catastrophic collapse of stratovolcanoes induced by gradual volcanic spreading. *Nature* 387:387–90

Van Wyk de Vries B, Merle O. 1996. The effect of volcanic constructs on rift fault patterns. *Geology* 24(7):643–46

Voight B. 1981. Time scale for the first moments of the May 18 eruption. *The 1980 Eruptions of Mount St. Helens, Washington. U.S. Geol. Survey Prof. Pap.* 1250:69–86

Voight B, Elsworth D. 1997. Failure of volcano slopes. *Geotechnique* 47:1–31

Wyss M. 1988. A proposed source model for the Great Kau, Hawaii, earthquake of 1868. *Bull. Seis. Soc. Am.* 78:1450–62

Annual Review of Earth and Planetary Science
Volume 28, 2000

CONTENTS